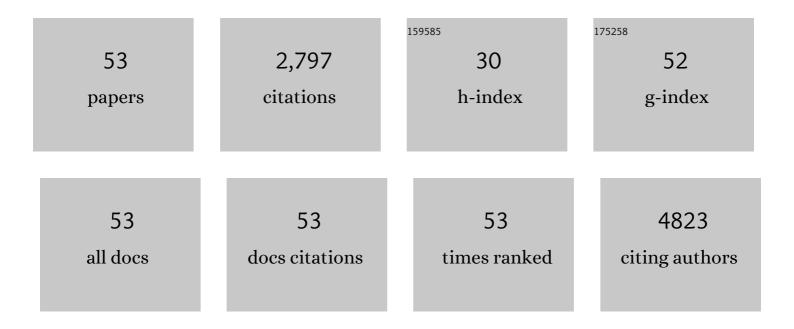
Qiuming Yu

List of Publications by Year in descending order

Source: https://exaly.com/author-pdf/3545359/publications.pdf Version: 2024-02-01



#	Article	IF	CITATIONS
1	Inverted Size-Dependence of Surface-Enhanced Raman Scattering on Gold Nanohole and Nanodisk Arrays. Nano Letters, 2008, 8, 1923-1928.	9.1	360
2	Quantitative and simultaneous detection of four foodborne bacterial pathogens with a multi-channel SPR sensor. Biosensors and Bioelectronics, 2006, 22, 752-758.	10.1	274
3	Hierarchical zwitterionic modification of a SERS substrate enables real-time drug monitoring in blood plasma. Nature Communications, 2016, 7, 13437.	12.8	156
4	Multifunctional magnetic–plasmonic nanoparticles for fast concentration and sensitive detection of bacteria using SERS. Biosensors and Bioelectronics, 2012, 31, 130-136.	10.1	123
5	Surface functionalization for self-referencing surface plasmon resonance (SPR) biosensors by multi-step self-assembly. Sensors and Actuators B: Chemical, 2003, 90, 22-30.	7.8	116
6	Sensitive and Fast Detection of Fructose in Complex Media via Symmetry Breaking and Signal Amplification Using Surface-Enhanced Raman Spectroscopy. Analytical Chemistry, 2014, 86, 2387-2394.	6.5	94
7	Solution-processed visible-blind UV-A photodetectors based on CH ₃ NH ₃ PbCl ₃ perovskite thin films. Journal of Materials Chemistry C, 2017, 5, 3796-3806.	5.5	90
8	Probing the Protein Orientation on Charged Self-Assembled Monolayers on Gold Nanohole Arrays by SERS. Langmuir, 2007, 23, 8659-8662.	3.5	89
9	Stealth Surface Modification of Surface-Enhanced Raman Scattering Substrates for Sensitive and Accurate Detection in Protein Solutions. ACS Nano, 2015, 9, 2668-2676.	14.6	89
10	Surfaceâ€Enhanced Raman Scattering for Rapid Detection and Characterization of Antibioticâ€Resistant Bacteria. Advanced Healthcare Materials, 2018, 7, e1701335.	7.6	85
11	Surface-enhanced Raman scattering on gold quasi-3D nanostructure and 2D nanohole arrays. Nanotechnology, 2010, 21, 355301.	2.6	77
12	Ultra-low fouling and high antibody loading zwitterionic hydrogel coatings for sensing and detection in complex media. Acta Biomaterialia, 2016, 40, 31-37.	8.3	77
13	Solvent-molecule-mediated manipulation of crystalline grains for efficient planar binary lead and tin triiodide perovskite solar cells. Nanoscale, 2016, 8, 7621-7630.	5.6	65
14	Plasmonic Gold Nanohole Array for Surface-Enhanced Raman Scattering Detection of DNA Methylation. ACS Sensors, 2019, 4, 1534-1542.	7.8	65
15	Organic Ultraviolet Photodetectors Exhibiting Photomultiplication, Low Dark Current, and High Stability. Advanced Materials Technologies, 2017, 2, 1700025.	5.8	61
16	Multi-functional, thiophenol-based surface chemistry for surface-enhanced Raman spectroscopy. Chemical Communications, 2017, 53, 4550-4561.	4.1	57
17	Inverted hybrid solar cells based on pyrite FeS2 nanocrystals in P3HT:PCBM with enhanced photocurrent and air-stability. Solar Energy Materials and Solar Cells, 2013, 116, 252-261.	6.2	49
18	Paper Sensor Coated with a Poly(carboxybetaine)-Multiple DOPA Conjugate via Dip-Coating for Biosensing in Complex Media. Analytical Chemistry, 2017, 89, 10999-11004.	6.5	49

QIUMING YU

#	Article	IF	CITATIONS
19	Structure of Cathodically Deposited Nickel Hexacyanoferrate Thin Films Using XRD and EXAFS. Langmuir, 2002, 18, 7714-7721.	3.5	47
20	Tailoring Plasmonic Nanostructures for Optimal SERS Sensing of Small Molecules and Large Microorganisms. Small, 2011, 7, 371-376.	10.0	46
21	Functionalized plasmonic nanostructure arrays for direct and accurate mapping extracellular pH of living cells in complex media using SERS. Biosensors and Bioelectronics, 2015, 73, 202-207.	10.1	44
22	Understanding the effects of dielectric medium, substrate, and depth on electric fields and SERS of quasi-3D plasmonic nanostructures. Optics Express, 2011, 19, 20493.	3.4	42
23	Flexible Narrowband Ultraviolet Photodetectors with Photomultiplication Based on Wide Band Gap Conjugated Polymer and Inorganic Nanoparticles. ACS Applied Materials & Interfaces, 2018, 10, 24064-24074.	8.0	40
24	Anisotropic Growth of Iron Pyrite FeS ₂ Nanocrystals via Oriented Attachment. Chemistry of Materials, 2015, 27, 3516-3525.	6.7	39
25	In Situ Strain-Level Detection and Identification of <i>Vibrio parahaemolyticus</i> Using Surface-Enhanced Raman Spectroscopy. Analytical Chemistry, 2013, 85, 2630-2637.	6.5	38
26	Sensitive Bacterial Detection via Dielectrophoretic-Enhanced Mass Transport Using Surface-Plasmon-Resonance Biosensors. Analytical Chemistry, 2018, 90, 14635-14642.	6.5	37
27	Light Transmission and Surface-Enhanced Raman Scattering of Quasi-3D Plasmonic Nanostructure Arrays with Deep and Shallow Fabry-Pérot Nanocavities. Journal of Physical Chemistry C, 2011, 115, 10996-11002.	3.1	34
28	Controlling morphology and phase of pyrite FeS2 hierarchical particles via the combination of structure-direction and chelating agents. CrystEngComm, 2012, 14, 4188.	2.6	34
29	Controlled colloidal synthesis of iron pyrite FeS ₂ nanorods and quasi-cubic nanocrystal agglomerates. Nanoscale, 2014, 6, 1029-1037.	5.6	34
30	Impact of cesium on the phase and device stability of triple cation Pb–Sn double halide perovskite films and solar cells. Journal of Materials Chemistry A, 2018, 6, 17426-17436.	10.3	33
31	High efficiency PTB7-based inverted organic photovoltaics on nano-ridged and planar zinc oxide electron transport layers. Journal of Materials Chemistry A, 2015, 3, 5563-5571.	10.3	32
32	Narrowband Ultraviolet Photodetectors Based on Nanocomposite Thin Films with High Gain and Low Driving Voltage. ACS Applied Materials & Interfaces, 2018, 10, 41552-41561.	8.0	31
33	Label-Free Raman Observation of TET1 Protein-Mediated Epigenetic Alterations in DNA. Analytical Chemistry, 2019, 91, 7304-7312.	6.5	23
34	Tunable and highly reproducible surface-enhanced Raman scattering substrates made from large-scale nanoparticle arrays based on periodically poled LiNbO3templates. Science and Technology of Advanced Materials, 2013, 14, 055011.	6.1	20
35	Tuning cesium–guanidinium in formamidinium tin triiodide perovskites with an ethylenediammonium additive for efficient and stable lead-free perovskite solar cells. Materials Advances, 2020, 1, 3507-3517.	5.4	20
36	Optofluidic microsystem with quasi-3 dimensional gold plasmonic nanostructure arrays for online sensitive and reproducible SERS detection. Analytica Chimica Acta, 2015, 863, 41-48.	5.4	19

QIUMING YU

#	Article	IF	CITATIONS
37	Surface-Enhanced Raman Scattering on Gold Nanohole Arrays in Symmetrical Dielectric Environments Exhibiting Electric Field Extension. Journal of Physical Chemistry C, 2016, 120, 25519-25529.	3.1	19
38	Inverted hybrid CdSe–polymer solar cells adopting PEDOT:PSS/MoO ₃ as dual hole transport layers. Physical Chemistry Chemical Physics, 2016, 18, 3463-3471.	2.8	18
39	Tuning the spectral response of ultraviolet organic–inorganic hybrid photodetectors <i>via</i> charge trapping and charge collection narrowing. Physical Chemistry Chemical Physics, 2018, 20, 11273-11284.	2.8	18
40	Tuning multiple Fano and plasmon resonances in rectangle grid quasi-3D plasmonic-photonic nanostructures. Applied Physics Letters, 2013, 103, 053117.	3.3	17
41	Design and development of plasmonic nanostructured electrodes for ITO-free organic photovoltaic cells on rigid and highly flexible substrates. Nanotechnology, 2017, 28, 165401.	2.6	17
42	Long-range surface plasmon resonance and surface-enhanced Raman scattering on X-shaped gold plasmonic nanohole arrays. Physical Chemistry Chemical Physics, 2017, 19, 24126-24134.	2.8	17
43	X-shaped quasi-3D plasmonic nanostructure arrays for enhancing electric field and Raman scattering. Nanotechnology, 2012, 23, 405201.	2.6	16
44	Chemical Polymerization of Hydroxymethyl and Chloromethyl Functionalized PEDOT:PSS. ACS Applied Polymer Materials, 2019, 1, 3103-3114.	4.4	16
45	Manipulation of PEDOT:PSS with Polar and Nonpolar Solvent Post-treatment for Efficient Inverted Perovskite Solar Cells. ACS Applied Energy Materials, 2020, 3, 9656-9666.	5.1	16
46	Hydroxymethyl-Functionalized PEDOT-MeOH:PSS for Perovskite Solar Cells. ACS Applied Materials & Interfaces, 2020, 12, 17571-17582.	8.0	13
47	In situ controlled growth of well-dispersed Au nanoparticles inside the channels of SBA-15 using a simple, bio-inspired method for surface-enhanced Raman spectroscopy. RSC Advances, 2013, 3, 10154.	3.6	12
48	Plasmonic Aluminum Nanohole Arrays as Transparent Conducting Electrodes for Organic Ultraviolet Photodetectors with Bias-Dependent Photoresponse. ACS Applied Nano Materials, 2019, 2, 4942-4953.	5.0	12
49	Revealing Stability of Inverted Planar MA-Free Perovskite Solar Cells and Electric Field-Induced Phase Instability. Journal of Physical Chemistry C, 2020, 124, 18805-18815.	3.1	11
50	Ruddlesden–Popper Perovskites with Narrow Phase Distribution for Air‣table Solar Cells. Solar Rrl, 2022, 6, .	5.8	4
51	Optical properties and surface-enhanced Raman scattering of quasi-3D gold plasmonic nanostructures. Proceedings of SPIE, 2010, , .	0.8	1
52	Incorporating Aluminum Plasmonic Nanohemisphere Arrays into Organic Ultraviolet Photodetectors for Improved Photoresponse. ACS Applied Nano Materials, 2019, 2, 6690-6700.	5.0	1
53	The Fano resonance in quasi-3D gold plasmonic nanostructure arrays for surface-enhanced Raman scattering. Proceedings of SPIE, 2012, , .	0.8	0